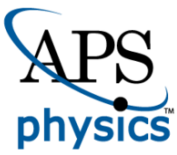

General-relativistic simulations of black-hole–neutron-star mergers: Effects of tilted magnetic fields

Zachariah B. Etienne, Vasileios Paschalidis, and Stuart L. Shapiro

Phys. Rev. D **86**, 084026 — Published 9 October 2012

DOI: 10.1103/PhysRevD.86.084026

General relativistic simulations of black hole-neutron star mergers: Effects of tilted magnetic fields

Zachariah B. Etienne[1], Vasileios Paschalidis[1], and Stuart L. Shapiro[1,2]
[1] *Department of Physics, University of Illinois at Urbana-Champaign, Urbana, IL 61801*
[2] *Department of Astronomy and NCSA, University of Illinois at Urbana-Champaign, Urbana, IL 61801*

Black hole–neutron star (BHNS) binary mergers can form disks in which magnetorotational instability (MRI)-induced turbulence may drive accretion onto the remnant BH, supporting relativistic jets and providing the engine for a short-hard gamma-ray burst (SGRB). Our earlier study of magnetized BHNSs showed that NS tidal disruption winds the magnetic field into a toroidal configuration, with poloidal fields so weak that capturing MRI with full-disk simulations would require $\sim 10^8$ CPU-hours. In that study we imposed equatorial symmetry, suppressing poloidal magnetic fields that might be generated from plasma crossing the orbital plane. Here we show that initial conditions that break this symmetry (i.e., *tilted* poloidal magnetic fields in the NS) generate much stronger poloidal fields in the disk, indicating that asymmetric initial conditions may be necessary for establishing BHNS mergers as SGRB progenitors via fully general relativistic MHD simulations. We demonstrate that BHNS mergers may form an SGRB engine under the right conditions by seeding the remnant disk from an unmagnetized BHNS simulation with purely poloidal fields dynamically unimportant initially, but strong enough to resolve MRI. Magnetic turbulence occurs in the disk, driving accretion and supporting Poynting-dominated jet outflows sufficient to power an SGRB.

PACS numbers: 04.25.D-,04.25.dk,04.40.Nr

I. INTRODUCTION

At the end of a black hole–neutron star (BHNS) binary merger, the NS may tidally disrupt, forming a hot, massive disk around the BH, with the temperature, density, and collimated magnetic field profiles required to launch a jet and trigger a short-hard gamma-ray burst (SGRB).

Recently a suite of stationary BH+disk general relativistic MHD (GRMHD) simulations was performed, in which the disks were seeded with different magnetic field topologies and strengths [1]. It was found that to support a long-term, Poynting-dominated jet, sufficiently strong dipole poloidal fields are required in the disk initially.

This result may be problematic for BHNS mergers, because the NS tidal disruption event invariably winds the magnetic fields into a toroidal configuration in all magnetized BHNS simulations to date. For example, in [2], we performed the first parameter survey of magnetized BHNS mergers using fully general relativistic MHD simulations, varying the initial magnetic field strength and geometry, and the aligned BH spin. We seeded the NS with purely poloidal magnetic fields and found that after tidal disruption, the fluid motion becomes strongly toroidal during disk formation, dragging the magnetic field lines into a *predominantly toroidal* configuration, leaving very weak poloidal fields.

However, even these very weak poloidal fields can be exponentially amplified via the magnetorotational instability (MRI). But the weaker the poloidal fields, the shorter the wavelength of the fastest-growing MRI mode. Numerically, if this wavelength is not resolved by at least 10 gridpoints, MRI cannot be captured numerically [3]. We performed a local analysis of our magnetized BHNS disks formed in [2] and found that the fastest-growing MRI wavelength was under-resolved by about a factor of 10 on average. These simulations required about 30,000 CPU-hours and two weeks of wall-clock time, so resolving MRI would require about *300 million CPU-hours* and 20 weeks of wall-clock time, which is computationally unfeasible.

Resolving MRI is considerably more challenging in BHNS simulations than in typical magnetized NSNS simulations [4–8]. First, in NSNS mergers, the Kelvin-Helmholtz instability amplifies the poloidal magnetic field by an order of magnitude when the stars come in contact [4, 5]. Second, in BHNS mergers, the NS core containing most of the magnetic energy is quickly swallowed by the BH following tidal disruption, leaving only weakly magnetized matter in the outer layers to form a disk which is more extended than disks formed in NSNS mergers. Third, frame-dragging in BHNS mergers enhances the winding of the magnetic field, reducing the poloidal component even further. The net effect is that the wavelength of the fastest-growing MRI mode is much smaller in merging BHNSs than NSNSs with the same initial magnetized NS.

In previous magnetized BHNS simulations [2, 9], weak poloidal fields in the remnant disk made it impossible to resolve MRI-induced turbulence, which would drive accretion, and possibly launch and sustain jets. Additionally, in our earlier study the system obeyed equatorial symmetry, which saved computational cost. However, these symmetric configurations prevent plasma motion across the orbital plane and thus poloidal magnetic fields that might be generated from such motion. Therefore we hypothesize that *introducing asymmetries in this system will very likely enhance the poloidal fields in the remnant disk, possibly enabling us to capture MRI.* Such asymmetries may be common in nature, given the magnetic field misalignment of the double pulsar system PSR J0737-

3039 [10].

Here we seed the pre-disrupted NS with the same purely poloidal fields as our previous work, but also *break the symmetry* by tilting them relative to the orbital angular momentum. We find that as the tilt angle increases to 90°, poloidal fields in our remnant disk become stronger, confirming our hypothesis. But the resulting field strengths are not sufficient to resolve MRI, establish turbulence, or launch a jet.

The question then arises: could the presence of a dominant poloidal dipole field in the remnant BHNS disk produce an SGRB engine? To answer this, we seed the remnant disk from an unmagnetized BHNS simulation with a purely dipole poloidal field, dynamically unimportant initially, but strong enough to resolve MRI. Within a few orbital periods, turbulence sets in and above the BH poles the magnetic fields collimate and relativistic outflows turn on, sufficient to power an SGRB. This is the first GRMHD simulation to demonstrate that jets can be produced from a disk formed at the end of a BHNS merger for a suitable remnant field.

We conclude that strong dipole poloidal fields in the remnant disks from BHNS mergers can give rise to MRI and launch Poynting-dominated outflows. Forming such poloidal fields strong enough to resolve MRI self-consistently through GRMHD simulations will likely require asymmetric initial conditions.

The paper is structured as follows. In Sec. II we describe the initial data, basic evolution equations, and numerical methods. The basic results are presented in Sec. III and summarized in Sec. IV. Throughout this work, geometrized units are adopted, where $G = c = 1$, unless otherwise specified.

II. BASIC TECHNIQUE

Our simulation software and methods are the same as used for case B4 in [2], except for a few key improvements. First, in our vector potential formulation for the induction equation, we adopt the "Generalized Lorenz gauge" (GL) we developed in [11], choosing $1/\xi = 0.45M$. This modification results in *damped*, traveling EM gauge modes, preventing spurious B-fields from appearing on refinement boundaries more effectively than our original, undamped Lorenz gauge condition [2]. Second, we fixed a coding error introduced in our attempt to make the primitives solver more robust in [2]; this error affected only that study. The net effect of this error was a doubling of truncation errors, but ultimately it had no effect on the bulk dynamics of our simulations. After fixing them, for example, the small disk mass amplification and gravitational wave mismatch found in our previous work when comparing unmagnetized cases (A0 and B0) to the strongest magnetic field cases (A4 and B4) [2] are significantly reduced.

Finally, we no longer impose symmetry across the orbital plane, except in one of our simulations. Not imposing symmetry across the orbital plane enables us to study asymmetric magnetic field configurations. In this work, we apply a rotation matrix to the vector potential [Eqs. (11) & (12) of [2]] to tilt the purely poloidal magnetic fields 45° and 90° relative to the orbital angular momentum vector.

We have also added two new diagnostics to better monitor magnetic effects. The first diagnostic monitors the fastest-growing MRI wavelength [12],

$$\lambda_{\rm MRI} \approx 2\pi \frac{|v_{\theta,A}|}{|\Omega(r,\theta)|} \approx 2\pi \frac{\sqrt{|b_P b^P|/(b^2+\rho_b h)}}{|\Omega(r,\theta)|}, \qquad (1)$$

where $|b^P| \equiv \sqrt{b_\mu b^\mu - |b_\mu (e_{\hat\phi})^\mu|^2}$, and $(e_{\hat\phi})^\mu$ is the toroidal orthonormal vector carried by an observer comoving with the fluid. The second new diagnostic measures Poynting flux across a surface $\mathcal{S}$, $L_{\rm EM} \equiv -\int T_t^{r({\rm EM})}\sqrt{-g}dS$, where $T_\nu^{\mu({\rm EM})}$ is the electromagnetic stress-energy tensor.

III. RESULTS

Our initial data are generated using the conformal thin-sandwich (CTS) formulation [13–15], with the NS modeled as an irrotational, unmagnetized, $n = 1$ polytrope. The initial binary is in a quasi-equilibrium circular orbit just outside the tidal disruption radius, with the BH irreducible mass three times that of the isolated NS ADM mass. The BH spin parameter is set to $a/M = 0.75$, aligned with the orbital angular momentum (top-left frame of Fig. 1). As in [2], the BH and NS in our simulations are covered by 70 and 80 gridpoints on average across their shortest diameters, respectively. Our grid consists of 8 and 9 refinement boxes centered on the NS and BH, respectively, with outer boundary at $210M$.

We first evolve a total of five cases: B0, B4-0, B4-45, B4-90, and B4-0-Sym. B4-0-Sym, which imposes symmetry across the orbital plane, is identical to case B4 in [2], but is now evolved with our latest code. B4-0 is the same as B4-0-Sym but does not impose equatorial symmetry. B4-45 and B4-90 are the same as B4-0, but the initial poloidal NS magnetic fields are tilted by 45° and 90°, respectively. Finally, B0 is the same as B4-0, except with zero magnetic fields.

We evolve the unmagnetized NS for nearly four orbits before seeding its interior with a purely poloidal, $\sim 10^{16}$G magnetic field, in the magnetized cases. With average magnetic-to-gas pressure of 0.5%, these magnetic fields are dynamically unimportant to the NS. The second panel of Fig. 1 shows B4-90 when the magnetic fields are first seeded in the NS. Though a NS cannot stably maintain purely poloidal fields [16, 17], we choose such an initial configuration, together with a very high field amplitude, to maximize the prospect of obtaining large residual poloidal fields in the remnant disk, making it

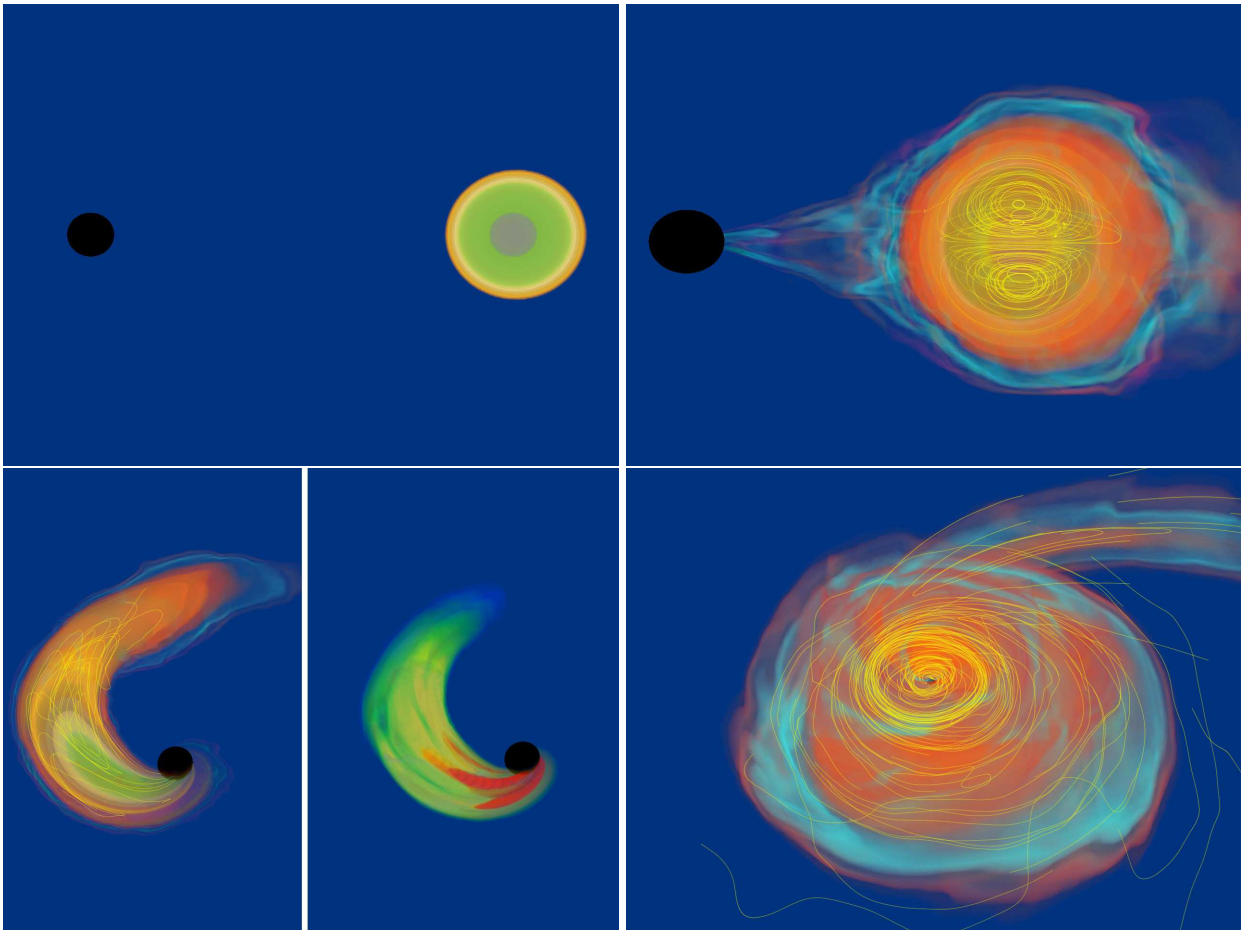

FIG. 1. Case B4-90 3D snapshots. Top-left: initial data, NS on the right (from highest to lowest rest-mass density, the colors are: grey, green, yellow, orange, red, and blue), BH apparent horizon (AH) on the left. Top-right: magnetic fields (yellow) are seeded into NS after ≈ 4 orbits (simulation time $t = 633M$). Bottom-left: tidal disruption after ≈ 5 orbits ($t = 882M$); density and magnetic field lines on the left, and magnetic energy density $b^2/2$ on the right (from highest to lowest $b^2/2$, the colors are: red, yellow, and green). Bottom-right: final disk density profile with magnetic field lines, about 33ms ($1.4M_\odot/M_0$) after disk formation ($t = 2072M$), where M_0 is the initial rest mass of the NS.

more computationally feasible to resolve the MRI (cf. Eq. 1).

The amplitude of the magnetic field seeds in the NS scales like the local gas pressure and is thus strongly peaked at the core of the NS. During tidal disruption, the core of the NS is accreted (bottom-left frame in Fig. 1), which would seem to leave very little magnetic energy available for the remnant disk. However, the tidal disruption of the orbiting NS stretches its frozen-in magnetic fields, leading to a net *amplification* of magnetic energy. The bottom frame of Fig. 2 demonstrates that midway through tidal disruption (accretion history is plotted in the top frame) the magnetic energy outside the AH peaks at ~ 2 times the initial value, then rapidly drops, so that the final disk has roughly the same magnetic energy as the initial seed magnetic fields.

After evolving the disks in cases B4-0, B4-45, B4-90, and B4-0-Sym for about $1200M$, 14% of the NS rest mass remains outside the AH, regardless of the presence or tilt of the magnetic field (see top panel of Fig. 2). If this mass were converted into gamma-rays at an efficiency of 1%, the energy output would be of order 10^{51}ergs, sufficient to launch an SGRB. However, for an SGRB to take place, models indicate that jets must be launched from the final disk, and jet-launching may fail to occur if the disk magnetic fields are not sufficiently dipolar and poloidal near the BH [1].

When we terminate B4-90, the disk magnetic fields are almost purely *toroidal* (lower-right frame of Fig. 1), and fluid *inflow* continues in the BH polar regions. MRI could amplify the remnant poloidal fields, but only if $\lambda_{\rm MRI}/\Delta x \gtrsim 10$, where Δx is the local gridspacing [3]. On average, this ratio is only ≈ 1 in the B4-0 and B4-0-Sym disks, as these cases are by construction equatorially symmetric. The ratio increases to ≈ 3 in B4-45 and to ≈ 8 in B4-90. Computational cost goes like $(\Delta x)^{-4}$ in these simulations, so MRI can be resolved in case B4-90 at about $(\frac{1}{10})^{-4}/(\frac{8}{10})^{-4} = 1/4096$ the cost of B4-0.

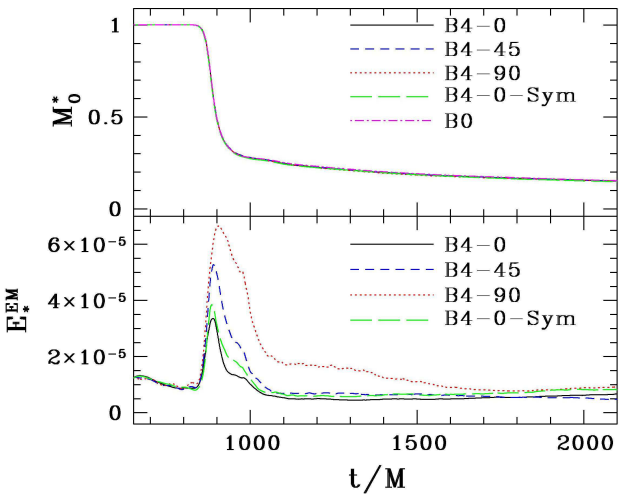

FIG. 2. Rest mass outside the AH M_0^* (top frame) and magnetic energy outside the AH $E_*^{\rm EM}$ (bottom frame), versus time. Rest mass and magnetic energy are given by Eqs. (23) and (13) in [2], respectively.

However, even though we are using high-resolution grids and very strong initial magnetic fields, we are still not able to capture MRI and its effects.

To demonstrate that BHNS mergers may form an SGRB engine under the *right* conditions, we evolve case B5, where we artificially seed case B0's final disk with a purely poloidal magnetic field having an average magnetic-to-gas pressure ratio of $\sim$ 0.1%, corresponding to average magnetic field strength of $\approx 10^{14}(1.4M_\odot/M_0)G$ (cf. B4-90's final disk, with $\approx 4\times10^{14}(1.4M_\odot/M_0)G$ average magnetic field strength). Though these magnetic fields are dynamically weak initially, they are strong enough to resolve MRI throughout most of the disk because they are purely poloidal. There are clear *inflows* above the BH poles when the disk is first seeded with magnetic fields (upper-left panel of Fig. 3). Within ~ 0.5 orbital periods magnetic turbulence begins, accretion of the dipole poloidal fields occurs, and the inflows diminish.

Though $b^2/(2\rho_0)$ is at most only $\sim 10^{-4}$ initially (Fig. 3, middle-left panel), after ~ 3 orbital periods, it amplifies to a maximum value of $\gtrsim 100$ in the Poynting-dominated funnels above and below the BH (middle-right panel), and mildly-relativistic *outflows* appear above and below the BH. For steady-state, Poynting-dominated jets, the energy-to-mass flux ratio [which can be shown to be $\approx b^2/(2\rho_0)$] is equal to the maximum possible Lorentz factor in the (asymptotic) jet [18]. However, in general, the actual terminal Lorentz factor of the jet is reduced by the (neutrino-induced) baryon-loading into the jet funnel [19–21]. But, the Blandford-Znajek process [22], which is captured in our simulations, alone can accelerate a Poynting-dominated jet to the necessary Lorentz factors even in the presence of baryon loading [23]. In fact, magnetic launching of ultrarelativistic polar outflows from a BH-disk system is possible even for nonspinning BHs provided the neutrino luminosity $L_\nu \lesssim 10^{52}$ergs/sec [19]. Newtonian simulations of (10:1 mass-ratio) BHNS mergers find characteristic neutrino luminosities $L_\nu \sim 10^{51}$ergs/sec [24]. Moreover, neutron-rich outflows may result naturally in a high proton Lorentz factor [25]. Thus, we expect that jets formed following BHNS mergers can attain high Lorentz factors even when accounting for baryon-loading in the jet.

When we terminate the B5 simulation, the Poynting luminosity is $3.5\times10^{-3}\dot{M}_0c^2 = 1.28\times10^{52}$ergs/sec, which may be sufficient to power an SGRB. We terminated the simulation when densities in the funnel region began to drop below our atmospheric density. At the time of termination, $b^2/(2\rho_0)$ and the Poynting luminosity were still increasing. The final magnetic fields are turbulent in the disk (bottom-left panel Fig. 3), and form a large-scale helical structure along the BH spin axis (bottom panel).

IV. SUMMARY AND FUTURE WORK

In conclusion, if the NS tidally disrupts in a BHNS merger, its internal magnetic fields are wound by the fluid motion into a predominantly toroidal configuration. However, even very weak residual poloidal fields in the disk may be exponentially amplified by MRI, generating turbulence that drives accretion, ultimately launching jets and providing the engine for an SGRB.

Replicating this complete scenario with fully general relativistic MHD simulations has been impossible, since numerically resolving MRI in disks with such weak residual poloidal fields has been computationally unfeasible. In our earlier work, equatorial symmetry was imposed, which prevents poloidal fluid motion across the orbital plane, thus suppressing any poloidal magnetic fields that could be generated from this motion.

In this work, we no longer impose this symmetry and, in addition, choose asymmetric initial magnetic field configurations in the NS, tilting its poloidal fields with respect to the orbital angular momentum. Such asymmetries may be common, given the magnetic field misalignment of PSR J0737-3039. We find that the more the fields are tilted, the stronger the poloidal fields in the disk. When the initial magnetic fields are tilted 90°, the poloidal fields in the remnant disk are amplified by about a factor of 8, producing significantly more favorable conditions for modeling MRI. Our "Generalized Lorenz" gauge condition prevents the spurious growth of magnetic fields that may plague some AMR simulations that use a simpler "algebraic gauge" [26]. Adopting GL, we find that MRI is not resolvable with our chosen resolution and initial magnetized BHNS models, even when the initial fields are purely poloidal and have high amplitude.

To demonstrate that BHNS mergers may form an SGRB engine under the right conditions, we perform the first simulation that generates an SGRB engine from a

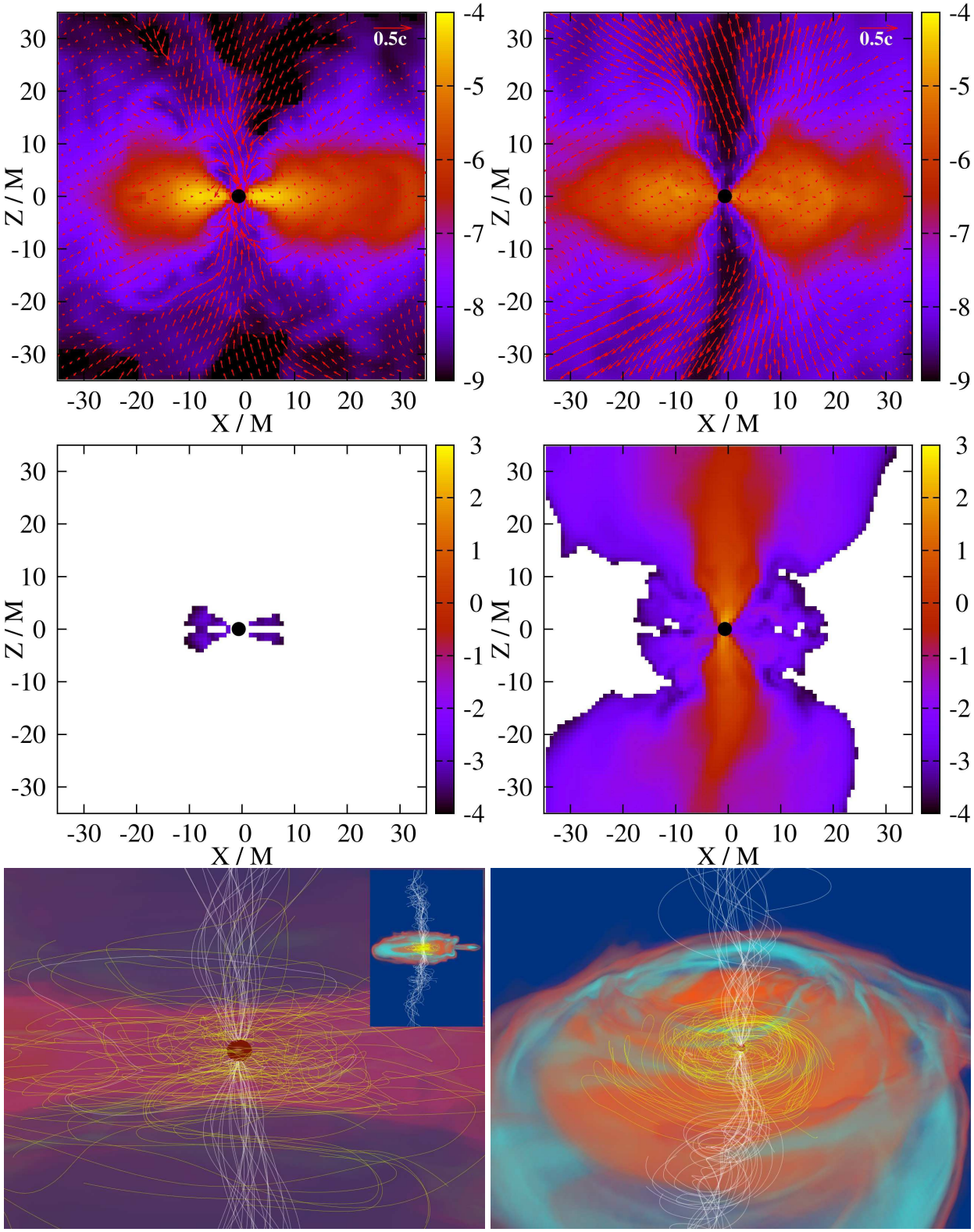

FIG. 3. Case B5 snapshots. Top row: map of $\log_{10}\rho_0$ on the meridional plane that passes through the BH centroid, at the time when the disk is seeded ($t = 2152M$) with magnetic fields (left frame) and when we terminated the simulation at $t = 2598M$ (right frame). Velocity arrows projected onto this plane are also displayed (red arrows). The initial central density of the NS is 9×10^{14}g cm$^{-3}(1.4M_\odot/M_0)^2$ (0.13 on the color bar), where M_0 is the initial NS rest mass. Middle row: map of $\log_{10} b^2/(2\rho_0)$ on the same meridional slices and times as the frames directly above them. Bottom row: 3D snapshots when we terminate the simulation, with viewing angles in the disk plane, both zoomed-in (left frame) and zoomed-out (left frame inset), and above the disk plane (right frame). Magnetic field streamlines emerging just above and below the BH poles are shown in white, and those in the disk are shown in yellow.

BHNS remnant disk with a purely poloidal field, which is dynamically weak initially, but strong enough to adequately resolve MRI. We then observe magnetic turbulence, followed by the large-scale collimation of magnetic fields and mildly relativistic outflows perpendicular to the disk, sufficient to power an SGRB.

We conclude that strong dipole poloidal fields in the remnant disks from BHNS mergers can give rise to MRI and launch Poynting-dominated outflows. Forming poloidal fields strong enough to resolve MRI self-consistently through GRMHD simulations will likely require asymmetric initial conditions.

Future work will focus on exploring new regions of parameter space that may further increase the poloidal fields in the remnant disk and the chances for launching jets. First, we intend to perform simulations with more rapidly spinning BHs. With initial spin parameter 0.75, the BH completely swallows the strongly-magnetized NS core during merger, leaving only the weakly-magnetized outer layers in the disk. A faster spinning BH may result in a larger, more strongly magnetized disk. In addition, we plan to explore asymmetric configurations in which the BH spin is misaligned with the orbital angular momentum. Plasma in the resulting warped disk will have much stronger motion parallel to the BH spin axis, likely enhancing the poloidal fields and the possibility of establishing BHNS mergers as plausible SGRB progenitors through fully general relativistic MHD simulations.

ACKNOWLEDGMENTS

The authors wish to thank Y. T. Liu, B. Farris, C. F. Gammie, and N. Vlahakis for useful discussions. We also thank our REU team, including G. Colten, M. Jin, A. Kim, D. Kolschowsky, B. Taylor, and F. Walsh, for assistance in producing the 3D visualizations. These visualizations were created using the ZIB Amira software package [27], and we gratefully acknowledge ZIB for providing us a license license. This paper was supported in part by NSF Grants AST-1002667, and PHY-0963136 as well as NASA Grant NNX11AE11G at the University of Illinois at Urbana-Champaign. This work used XSEDE, which is supported by NSF grant number OCI-1053575.

[1] K. Beckwith, J. F. Hawley, and J. H. Krolik, Astrophys. J. **678**, 1180 (May 2008).
[2] Z. B. Etienne, Y. T. Liu, V. Paschalidis, and S. L. Shapiro, Phys. Rev. D **85**, 064029 (Mar. 2012).
[3] M. Shibata, Y. T. Liu, S. L. Shapiro, and B. C. Stephens, Phys. Rev. D **74**, 104026 (Nov. 2006).
[4] D. J. Price and S. Rosswog, Science **312**, 719 (May 2006).
[5] M. Anderson, E. W. Hirschmann, L. Lehner, S. L. Liebling, P. M. Motl, D. Neilsen, C. Palenzuela, and J. E. Tohline, Physical Review Letters **100**, 191101 (May 2008).
[6] Y. T. Liu, S. L. Shapiro, Z. B. Etienne, and K. Taniguchi, Phys. Rev. D **78**, 024012 (Jul. 2008).
[7] B. Giacomazzo, L. Rezzolla, and L. Baiotti, Phys. Rev. D **83**, 044014 (Feb. 2011).
[8] L. Rezzolla, B. Giacomazzo, L. Baiotti, J. Granot, C. Kouveliotou, and M. A. Aloy, Astrophys. J. Lett. **732**, L6 (May 2011).
[9] S. Chawla, M. Anderson, M. Besselman, L. Lehner, S. L. Liebling, *et al.*, Phys.Rev.Lett. **105**, 111101 (2010).
[10] M. Burgay, N. D'Amico, A. Possenti, R. N. Manchester, A. G. Lyne, B. C. Joshi, M. A. McLaughlin, M. Kramer, J. M. Sarkissian, F. Camilo, V. Kalogera, C. Kim, and D. R. Lorimer, Nature (London) **426**, 531 (Dec. 2003).
[11] B. D. Farris, R. Gold, V. Paschalidis, Z. B. Etienne, and S. L. Shapiro, ArXiv e-prints(Jul. 2012), arXiv:1207.3354 [astro-ph.HE].
[12] R. F. Penna, J. C. McKinney, R. Narayan, A. Tchekhovskoy, R. Shafee, and J. E. McClintock, Mon. Not. Roy. Astron. Soc. **408**, 752 (Oct. 2010).
[13] Z. B. Etienne, J. A. Faber, Y. T. Liu, S. L. Shapiro, K. Taniguchi, and T. W. Baumgarte, Phys. Rev. D **77**, 084002 (Apr. 2008).
[14] Z. B. Etienne, Y. T. Liu, S. L. Shapiro, and T. W. Baumgarte, Phys. Rev. D **79**, 044024 (Feb. 2009).
[15] T. W. Baumgarte and S. L. Shapiro, *Numerical Relativity: Solving Einstein's Equations on the Computer* (Cambridge University Press, Cambridge, 2010).
[16] P. D. Lasky, B. Zink, K. D. Kokkotas, and K. Glampedakis, Astrophys. J. Lett. **735**, L20 (Jul. 2011).
[17] R. Ciolfi, S. K. Lander, G. M. Manca, and L. Rezzolla, Astrophys. J. Lett. **736**, L6 (Jul. 2011).
[18] N. Vlahakis and A. Königl, Astrophys. J. **596**, 1080 (Oct. 2003).
[19] A. Levinson, Astrophys. J. **648**, 510 (Sep. 2006).
[20] B. D. Metzger, T. A. Thompson, and E. Quataert, Astrophys. J. **659**, 561 (Apr. 2007).
[21] L. Lehner, C. Palenzuela, S. L. Liebling, C. Thompson, and C. Hanna, ArXiv e-prints(Dec. 2011), arXiv:1112.2622 [astro-ph.HE].
[22] R. D. Blandford and R. L. Znajek, Mon. Not. Roy. Astron. Soc. **179**, 433 (May 1977).
[23] J. C. McKinney, ArXiv Astrophysics e-prints(Jun. 2005), arXiv:astro-ph/0506368.
[24] S. Rosswog, Astrophys. J. **634**, 1202 (Dec. 2005).
[25] S. Razzaque and P. Mészáros, Astrophys. J. **650**, 998 (Oct. 2006).
[26] Z. B. Etienne, V. Paschalidis, Y. T. Liu, and S. L. Shapiro, Phys. Rev. D **85**, 024013 (Jan. 2012).
[27] D. Stalling, M. Westerhoff, and H.-C. Hege, in *The Visualization Handbook; Amira: A Highly Interactive System for Visual Data Analysis*, edited by C. D. Hansen and C. R. Johnson (Elsevier, 2005) Chap. 38, pp. 749–767, ISBN 978-0-12-387582-2.